Zhang *et al. Soft Sci.* **2025**, *5*, 9
DOI: 10.20517/ss.2024.72

Soft Science

Research Article

Open Access

Check for updates

Strong and tough polyvinyl alcohol hydrogels with high intrinsic thermal conductivity

Junliang Zhang[1,#], Chenyang Tang[1,#], Qingqing Kong[1], Mukun He[1], Peng Lv[2], Hua Guo[1], Yongqiang Guo[1], Xuetao Shi[1], Junwei Gu[1,*]

[1]Shaanxi Key Laboratory of Macromolecular Science and Technology, School of Chemistry and Chemical Engineering, Northwestern Polytechnical University, Xi'an 710072, Shaanxi, China.
[2]School of Materials Science and Engineering, Shandong University of Technology, Zibo 255000, Shandong, China.
[#]Authors contributed equally.

[*]**Correspondence to:** Prof. Junwei Gu, Shaanxi Key Laboratory of Macromolecular Science and Technology, School of Chemistry and Chemical Engineering, Northwestern Polytechnical University, 127 West Youyi Road, Beilin District, Xi'an 710072, Shaanxi, China. E-mail: gjw@nwpu.edu.cn

How to cite this article: Zhang, J.; Tang, C.; Kong, Q.; He, M.; Lv, P.; Guo, H.; Guo, Y.; Shi, X.; Gu, J. Strong and tough polyvinyl alcohol hydrogels with high intrinsic thermal conductivity. *Soft Sci.* **2025**, *5*, 9. https://dx.doi.org/10.20517/ss.2024.72

Received: 9 Dec 2024 **First Decision:** 3 Jan 2025 **Revised:** 17 Jan 2025 **Accepted:** 23 Jan 2025 **Published:** 26 Jan 2025

Academic Editor: Wei Hong **Copy Editor:** Pei-Yun Wang **Production Editor:** Pei-Yun Wang

Abstract

Although polyvinyl alcohol (PVA) hydrogels display huge potential in tissue engineering, flexible and wearable electronic devices and soft robotics, their low intrinsic thermal conductivity and weak mechanical properties severely limit their wider applications in these areas. Herein, a Hofmeister effect-assisted "directional freezing-stretching" tactic is employed for simultaneously enhancing the intrinsic thermal conduction and mechanical properties of PVA hydrogels. The hydrogels are obtained through directional freezing followed by salting-out treatment and subsequent mechanical stretching and salting-out (DFS). The DFS PVA hydrogel with 15 wt% of PVA and a stretching ratio of 4 (DFS4) exhibits the highest thermal conductivity of 1.25 W/(m·K), which is 2.4 and 2.8 times that of PVA hydrogel prepared through frozen-thawed (FT) [0.52 W/(m·K)] and frozen-salted out (FS) [0.45 W/(m·K)] methods, respectively. The DFS4 PVA hydrogel also possesses greatly improved mechanical performances, exhibiting an elongation at break of 163.1%. In addition, the tensile strength, toughness, and elastic modulus of DFS4 PVA hydrogel significantly increase to 27.1 MPa, 25.3 $MJ \cdot m^{-3}$, and 21.5 MPa from 0.4 MPa, 0.32 $MJ \cdot m^{-3}$, and 0.07 MPa for FT PVA hydrogels, respectively. It is elucidated that the salting-out effect generates hydrophobic and crystalline regions, while directional freezing and stretching enhance the chain orientation in the DFS strategy. These effects synergistically contribute to the improvement of thermal conductivity and mechanical properties of PVA hydrogels.

Keywords: Intrinsic thermal conductivity, polyvinyl alcohol hydrogels, directional freezing, salting-out, Hofmeister effect

INTRODUCTION

Hydrogels comprise a three-dimensional polymer network structure that is super hydrophilic and exhibits adaptable intriguing chemical and physical characteristics[1-4]. Polyvinyl alcohol (PVA) hydrogels display exceptional viscoelasticity, softness, chemical stability, biodegradability, and biocompatibility over other hydrogels, which endow them with immense potential for applications in fields such as tissue engineering, soft robotics, flexible electronics, and wearable electronic devices[5-10]. Due to the integration and multifunctionalization of flexible electronics and wearable electronic devices, the energy consumption of electronic components increases, leading to rapid accumulation of heat within the devices[11-15]. Therefore, the lifespan and stability of the devices will be decreased, necessitating the utilization of flexible electronic substrates with high efficiency of heat dissipation[16-18]. Furthermore, substrates for flexible electronic devices and wearable equipment must possess super flexibility, stretchability, and robust mechanical properties to meet the operational demands in dynamic shape-changing and strain-inducing environments[19-21].

However, conventional PVA hydrogels are characterized by a disordered arrangement and weak chain interactions within the polymer network, leading to significant phonon scattering and consequently a low thermal conductivity (λ) of approximately ~0.5 W/(m·K)[22,23]. Additionally, PVA hydrogels exhibit low crystallinity, with polymer chains aggregating through disordered entanglement and hydrogen bonding interactions, resulting in poor mechanical properties[24,25]. Therefore, the development of PVA hydrogels with superior λ and mechanical performances could significantly broaden their applications in the realms of flexible electronics and wearable electronic devices[26,27]. Despite this, most studies have solely focused on either their thermal conduction or mechanical properties[28-30], as achieving PVA hydrogels simultaneously with high intrinsic λ and superior mechanical properties remains a considerable challenge.

Research has unveiled that enhancing the crystallinity and orientation of the polymer network could facilitate thermal flow along the ordered molecular chains, thus effectively mitigating phonon scattering during the heat transfer process and improving the thermal conduction capability[31-35]. Uetani *et al.* induced the orientation of bacterial cellulose (BC) hydrogels through mechanical stretching[36]. The fabricated BC film demonstrated an enhanced intrinsic λ of 2.1 from 1.3 W/(m·K). Wu *et al.* investigated the λ of polyacrylamide (PAAM) hydrogels under different stretching ratios[37]. As the stretching ratio increased from 1 to 4, the λ of the PAAM hydrogel along the stretching direction enhanced from 0.75 to 1.4 W/(m·K).

Moreover, anisotropic structures, commonly found in nature, play a crucial role in certain natural load-bearing organizational structures[38]. Numerous studies have demonstrated that highly oriented structures are critical in achieving ultra-high mechanical strength[39-41]. Anisotropic hydrogels are widely prepared through directional freezing[42,43], mechanical stretching[44], or mechanical training[38] by transforming a disordered to an ordered structure so as to enhance their mechanical properties. In recent years, employing the Hofmeister effect[45,46], particularly the salting-out effect, has been recognized as an effective means to construct strong and tough hydrogels[10]. The salting-out ions (for instance, Cit^{3-} and SO_4^{2-}) would continuously drain water molecules from the space around polymer chains[47], leading to polymer aggregation, forming new hydrogen-bonding interactions between hydroxyl groups, and generating rigid cross-linking points[42]. For instance, Sun *et al.* applied a biomimetic "salting-out-alignment-locking" strategy to improve the mechanical performances of gelatin hydrogels via a combination of pre-stretching and salting-out effect[48]. The resulting hydrogel exhibited 940-, 2,830-, and 1,785-fold enhancement of tensile strength, modulus, and toughness, respectively. Very recently, Chen *et al.* proposed an "ordered-to-disordered" strategy to reconstruct the structure of PVA hydrogels employing the salting-out effect to

prepare super strong and tough PVA hydrogel fibers[39]. The PVA hydrogel fiber displayed an elongation at break of 257%, strength of 190.04 MPa, and toughness of 100.61 $MJ \cdot m^{-3}$, respectively. Inspired by the aforementioned studies, it would be reasonable to speculate that highly thermally conductive, strong, and tough PVA hydrogels can be afforded through the combination of the "salting out" effect and structural anisotropy.

In this work, we employed a Hofmeister effect-assisted strategy of "directional freezing-mechanical stretching" to improve the orientation of molecular chains within the PVA hydrogel network, fabricating high-strength, flexible, and highly thermally conductive hydrogels. This method involves the use of directional freezing to preferentially align the PVA molecular chains microscopically along the growth direction of ice crystals, while macroscopically fixing them into a specific shape. Subsequently, the hydrogel is mechanically stretched to alter the orientation of the PVA molecular chains along the stretching direction. Finally, the mechanically stretched PVA hydrogel is immersed into a sodium citrate (Na_3Cit) solution, facilitating the stabilization of anisotropic microstructure and the aggregation of PVA chains, to fabricate orderly oriented PVA hydrogels [Figure 1]. The effects of PVA content and structural anisotropy on the λ and mechanical properties of PVA hydrogels were systematically investigated. The developed PVA hydrogels are expected to demonstrate extensive potential for utilization in the fields of bioengineering, soft robotics, and flexible electronics.

EXPERIMENTAL

Materials

PVA (molecular weight ~75,000 g/mol, alcoholysis ~98%-99%), sodium citrate, and glutaraldehyde were purchased from Macklin Biochemical Technology Co., Ltd. Hydrochloric acid was provided by Sinopharm Chemical Reagent Co., Ltd. All chemicals were used as received without further treatment.

Characterizations and methods

Characterization details are provided in the Supplementary Materials.

Preparation of oriented PVA hydrogels

A certain amount of PVA and deionized water with predetermined mass ratios (5:95, 10:90, and 15:85, respectively) were added into a 100 mL three-necked flask. The PVA was allowed to swell in the mixture at room temperature for 30 min and stirred until homogeneous. It was then transferred to an oil bath of 90 °C to stir for an additional 2 h. The PVA solution was sonicated for 30 min to remove air bubbles, resulting in PVA solutions with mass fractions of 5 wt%, 10 wt%, and 15 wt% PVA, respectively.

The above PVA solutions were poured into a customized mold composed of a thermally conductive copper block at the bottom and a thermal-insulating polytetrafluoroethylene chamber at the top for directional freezing. Subsequently, the solutions were placed in a sodium citrate solution (1.5 mol/L) for salting out for 24 h, to obtain directional freezing-salting out PVA hydrogels (denoted as DFS PVA hydrogels). The DFS PVA hydrogels were then salted out in a sodium citrate solution (1.5 mol/L) for another 4 h, followed by stretching to two, three, and four times their original length at a rate of 10 mm/min using a universal testing machine, respectively. The stretched hydrogels were fixed using a mold and continued to be salted out in a sodium citrate solution (1.5 mol/L) for another 20 h, yielding oriented DFS PVA hydrogels, denoted as DFS2, DFS3, and DFS4, respectively. The DFS PVA hydrogel without stretching was denoted as DFS1. The preparation process of DFS PVA hydrogels is illustrated in Figure 1. PVA hydrogels were also prepared using frozen-thawed (FT) and frozen-salted out (FS) methods (described below) for comparison.

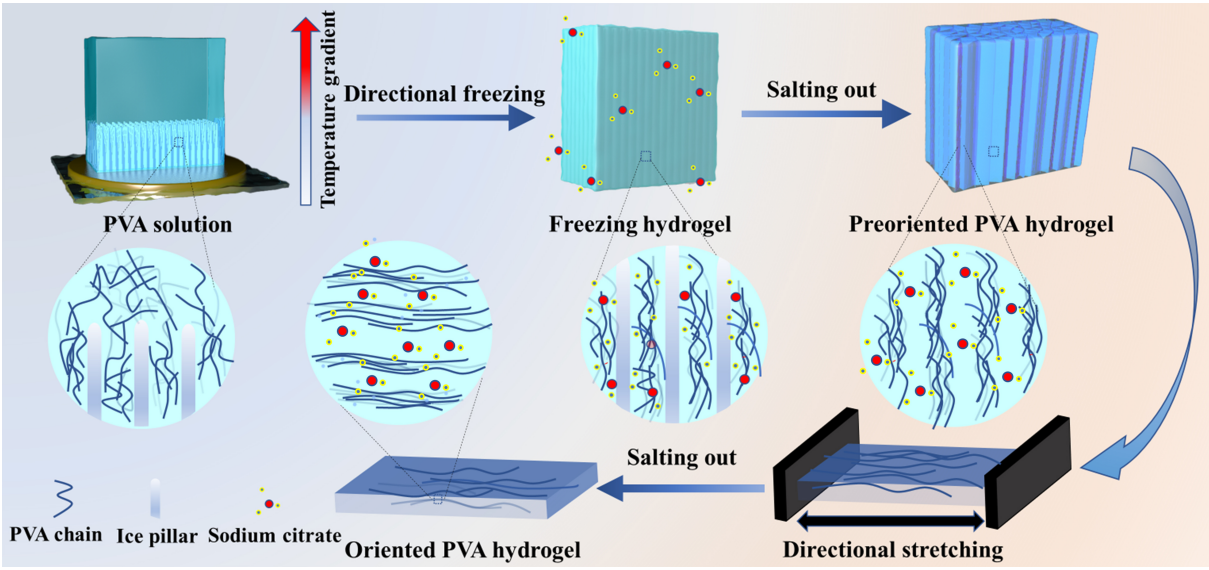

Figure 1. Schematic diagram for the preparation of oriented orderly PVA hydrogels with an anisotropic structure. PVA: Polyvinyl alcohol.

Preparation of FT PVA hydrogels

Aqueous PVA solutions with different mass fractions of PVA were poured into square glass molds and frozen at -18 °C for 12 h followed by thawing at room temperature for 2 h. The above procedure was repeated three times to afford the FT PVA hydrogels.

Preparation of FS PVA hydrogels

Aqueous PVA solutions with different mass fractions of PVA were poured into square glass molds and subjected to freezing at -18 °C for 12 h. After demolding, the samples were immersed in 100 mL of sodium citrate solution (1.5 mol/L) for salting out over 24 h to obtain FS PVA hydrogels.

RESULTS AND DISCUSSION

Structures and mechanisms of PVA hydrogels obtained by the DFS method

The morphologies of DFS PVA hydrogels were investigated and compared with those of FT and FS PVA hydrogels using scanning electron microscopy (SEM, Figure 2). As presented in Figure 2A, FT PVA hydrogels exhibited an isotropic and disordered structure. This is because PVA chains were squeezed and dispersed by disorderly growing ice crystals during the freezing and thawing process. Only a small amount of hydrogen bonds and physical entanglements existed between PVA chains, leading to the formation of disordered and loose three-dimensional structures of FT PVA hydrogels. The interior of FS PVA hydrogels presented a continuous porous structure, with uneven pore size and a wide distribution range [Figure 2B]. This is mainly due to the aggregation and disordered growth of PVA chains squeezed by ice crystals during the freezing and salting out process, resulting in the formation of disordered porous structures. In contrast, DFS1 PVA hydrogels displayed oriented pore channel structures, which aligned along the direction of ice crystal growth [Figure 2C]. As the stretching ratio increased from 2 to 4, the spacing between the pore channels decreased [Figure 2D-F]. Meanwhile, the pore channel walls became thinner and gradually transitioned into a tightly packed, long-range oriented continuous fibrous structure due to the tighter PVA chains caused by high stretching. Besides, the digital image of the DFS PVA hydrogel showed a dense arrangement along the stretching direction [Supplementary Figure 1].

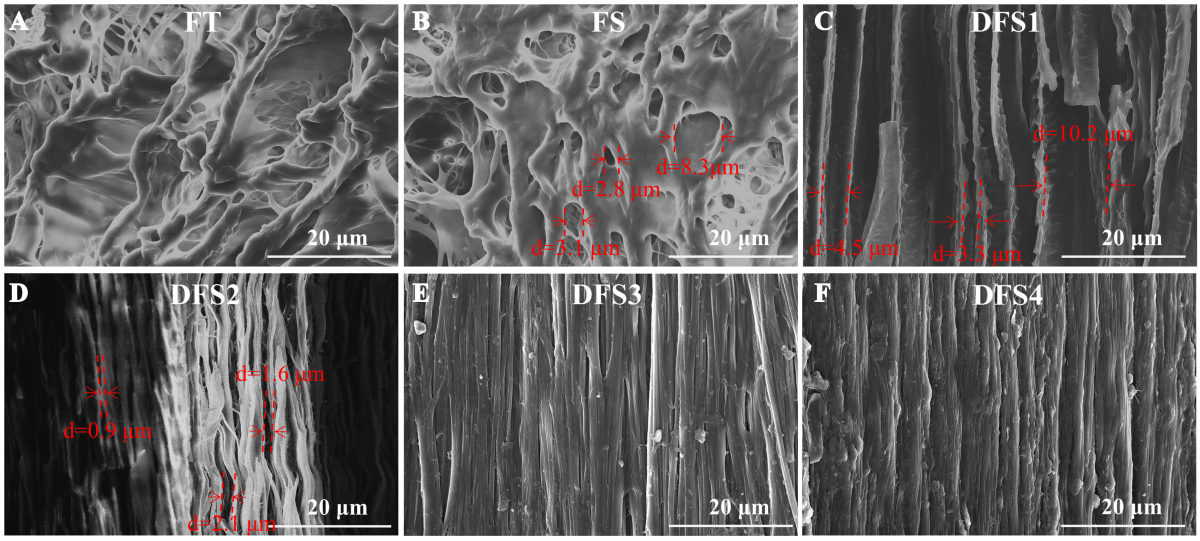

Figure 2. SEM images (longitudinal section) for FT (A), FS (B), and DFS PVA hydrogels with stretching ratios of 1 (C), 2 (D), 3 (E), and 4 (F) containing 15 wt% PVA. SEM: Scanning electron microscopy; FT: frozen-thawed; FS: frozen-salted out; DFS: directional freezing and salting-out; PVA: polyvinyl alcohol.

Fourier transform infrared (FT-IR) spectroscopy was then conducted to investigate the mechanisms of DFS methods. As observed in Figure 3A, all PVA hydrogels exhibited a characteristic absorption peak at around 3,292 cm^{-1} corresponding to the stretching vibration of O-H, implying that hydroxyl groups remained stable after the DFS method. However, this peak for FS and DFS PVA hydrogels with different stretching ratios shifted from 3,292 cm^{-1} to a lower wavenumber of 3,244 cm^{-1}, mainly attributed to the enhanced hydrogen bonding between PVA chains after salting-out [Figure 3B]. In addition, the intensity of the peak around 1,640 cm^{-1} corresponding to the shear bending vibration of -OH groups in water for FS PVA and DFS PVA hydrogels gradually decreased and shifted to a higher wavenumber [Figure 3C], indicating a reduction of water content within the PVA hydrogel during salting-out and disruption of hydrogen bonds between water molecules and PVA molecular chains[49]. Furthermore, a new characteristic peak at 1,144 cm^{-1} corresponding to the symmetric stretching vibration of O-C-C, which was the fingerprint peak of crystalline PVA chains, appeared for FS and DFS PVA hydrogels [Figure 3D]. Its intensity progressively increased with the stretching ratio, suggesting formation of crystalline regions during salting-out and stretching process[30]. Besides, FS and DFS PVA hydrogels showed enhanced characteristic peaks at 2,950, 1,420, and 1,092 cm^{-1} attributed to stretching vibrations of -CH, $-CH_2$ and C-O groups of PVA chains, respectively, indicating aggregation of the PVA chains and strong hydrophobic interaction after salting-out[50]. Additionally, the DFS hydrogels with different stretching ratios displayed very similar FT-IR spectra, suggesting the stretching was essentially a physical procedure.

In order to further investigate the effects of salting-out and mechanical stretching on the crystalline structure of PVA hydrogels, X-ray diffraction (XRD) and differential scanning calorimetry (DSC) analyses were conducted. As depicted in Figure 3E, FS and DFS PVA hydrogels exhibited new diffraction peaks at 21° and 41° compared to FT PVA hydrogels, which represented the (101) and (111) crystal plane, respectively, indicating crystalline domains existed in PVA hydrogels. Moreover, as the stretching ratio grew, the diffraction peak around 21° for DFS hydrogels gradually enhanced and the full width at half maximum broadened as shown in Supplementary Figure 2. This indicated an increase in the number of crystalline regions and a decrease in the average size of the crystallites. Analysis of DSC curves shown in Figure 3F revealed that FT PVA hydrogels exhibited the lowest crystallinity of 0.37%, which was lower than

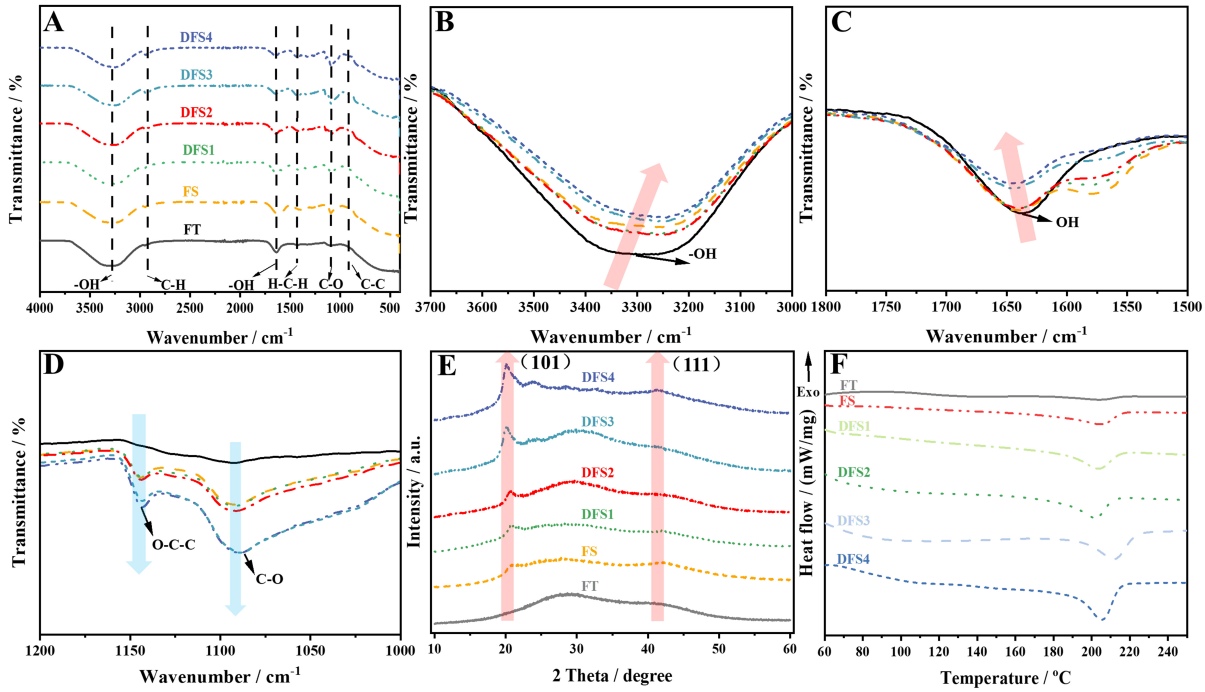

Figure 3. Full FT-IR spectra (A) and zoomed-in FT-IR spectra at 3,700-3,000 cm^{-1} (B), 1,800-1,500 cm^{-1} (C), and 1,200-1,000 cm^{-1} (D); XRD (E) and DSC (F) curves for FT PVA, FS PVA, and DFS PVA hydrogels. FT-IR: Fourier transform infrared; XRD: X-ray diffraction; DSC: differential scanning calorimetry; FT: frozen-thawed; PVA: polyvinyl alcohol; FS: frozen-salted out; DFS: directional freezing and salting-out.

that of FS PVA hydrogels (3.59%, Supplementary Figure 3). In the meantime, the DFS PVA hydrogels displayed higher crystallinity than both FT and FS PVA hydrogels, which increased from 4% to 11.97% as the stretching ratio increased from 1 to 4. This was consistent with the XRD results.

To conclude, the mechanism of the salting-out of the Hofmeister effect is as follows: the citrate anions would polarize the hydration water surrounding the PVA chains, disrupting the stability of hydrogen bonds between PVA and hydration water molecules. Meanwhile, the surface tension of cavities around the polymer chains increased, interfering with the hydrophobicity of the polymer. Macroscopically, the disordered aggregation and crystallinity of the hydrogel were enhanced, while microcosmically, the hydrogen bond between PVA molecules was strengthened. Salting out under a stretching state would generate hydrophobic domains, make the PVA chains crystallize in the orientation state, and strengthen the hydrogen bond between PVA chains in the amorphous region. Therefore, the orderly oriented alignment was locked due to the Hofmeister effect [Figure 4].

Small angle X-ray scattering (SAXS) was further employed to investigate the chain orientation of PVA polymers. As shown in Figure 5A, the 2D-SAXS pattern of FS PVA hydrogels displayed a uniformly distributed intensity ring, suggesting an isotropic structure. In contrast, the scattering circles of DFS PVA hydrogels were slowly distorted as the stretching ratio increased. The scattering patterns of the 2D-SAXS of DFS PVA hydrogels gradually transitioned from a circle of DFS1 to a distorted ellipse for DFS4, suggesting a highly anisotropic structure due to the orientation caused by stretching [Figure 5B-F]. Additionally, FS PVA hydrogels exhibited nearly the same scattering intensity in all directions. In contrast, the relative scattering intensity near the azimuthal angle of 90° for DFS PVA hydrogels increased with the stretching ratio [Figure 5G], suggesting enhanced anisotropy. The orientation degree of FS PVA hydrogels was only 0.359,

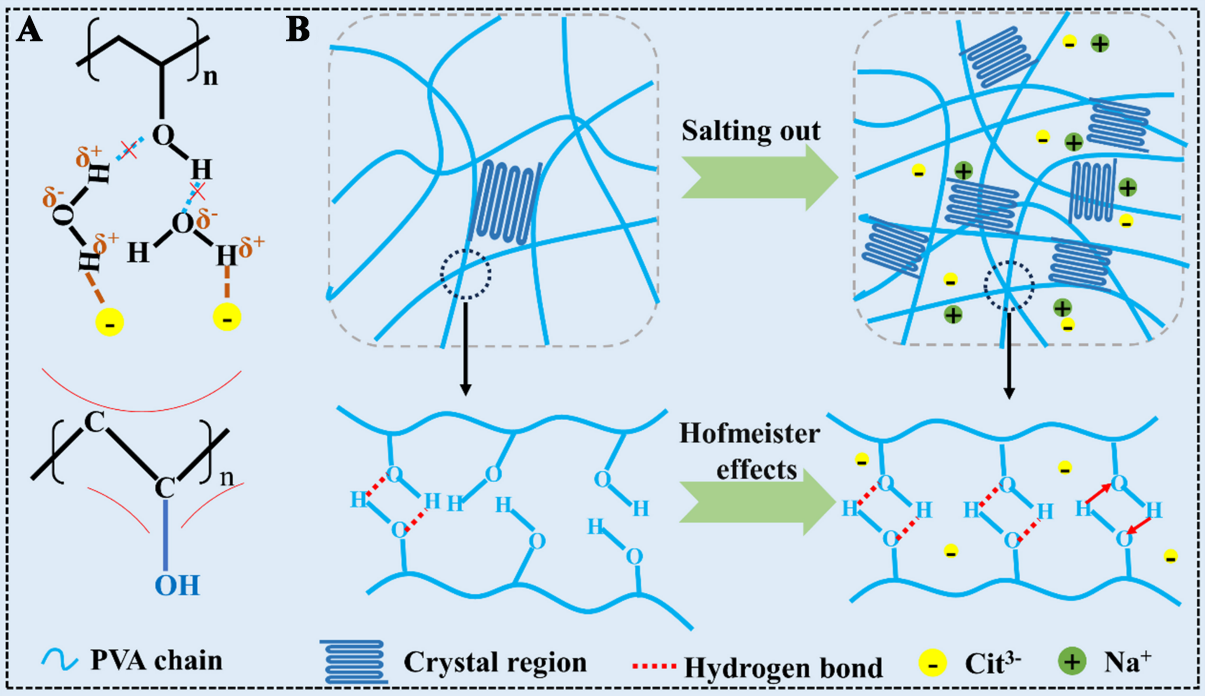

Figure 4. Schematics of the aggregation states of PVA hydrogel during the salting out process: the interactions among ions, polymer chains, and water molecules (A) and hydrogen bonds between PVA chains enhanced by Hofmeister effect (B). PVA: Polyvinyl alcohol.

while that of DFS PVA hydrogels increased from 0.580 to 0.839 as the stretching ratio rose from 1 to 4 [Figure 5H]. As depicted in Figure 5I, with increasing stretching, the diffraction peak representing the spacing between adjacent crystal domains in the corrected scattering intensity-scattering vector curve along the orientation direction shifted to the left, with a slight increase in peak intensity. This suggests that the average spacing between adjacent crystal domains expanded with greater stretching along the stretching direction. At a stretching ratio of 4, the DFS4 PVA hydrogel showed the largest crystal domain spacing along the orientation direction of 14.9 nm, higher than 9.9, 10.6, and 13.5 nm of DFS1, DFS2, and DFS3 PVA hydrogels, respectively [Figure 5J]. Additionally, the crystallinity of DFS PVA hydrogel enhanced as the stretching ratio increased, accompanied by a reduction in the average size of the crystalline domains [Supplementary Figures 2 and 3]. The average crystal size of DFS PVA hydrogel decreased, while the spacing between crystal domains expanded with increasing stretching, indicating that the curled molecular chains between the crystalline regions were straightened under mechanical stretching and that the molecular chains in the amorphous regions formed an ordered structure [Figure 5F].

Furthermore, the orderly oriented alignment was verified using a polarized optical microscope. As shown in Supplementary Figure 4, isotropic FS PVA hydrogels exhibited no birefringence at both 0° and 45°. In contrast, anisotropic DFS PVA hydrogels only displayed strong interference at 45° but not at 0°, further confirming their anisotropic structure.

Thermal conductivities of DFS PVA hydrogels

The λ was investigated to evaluate the thermal conduction performance of PVA hydrogels. As shown in Figure 6A, all the λ of FT, FS, and DFS1 PVA hydrogels decreased with increasing mass fraction of PVA. Besides, the FT PVA hydrogel exhibited the highest λ, followed by the λ of DFS1 PVA hydrogel, while the FS PVA hydrogel displayed the lowest λ at the same content of PVA. When the mass fraction of PVA was

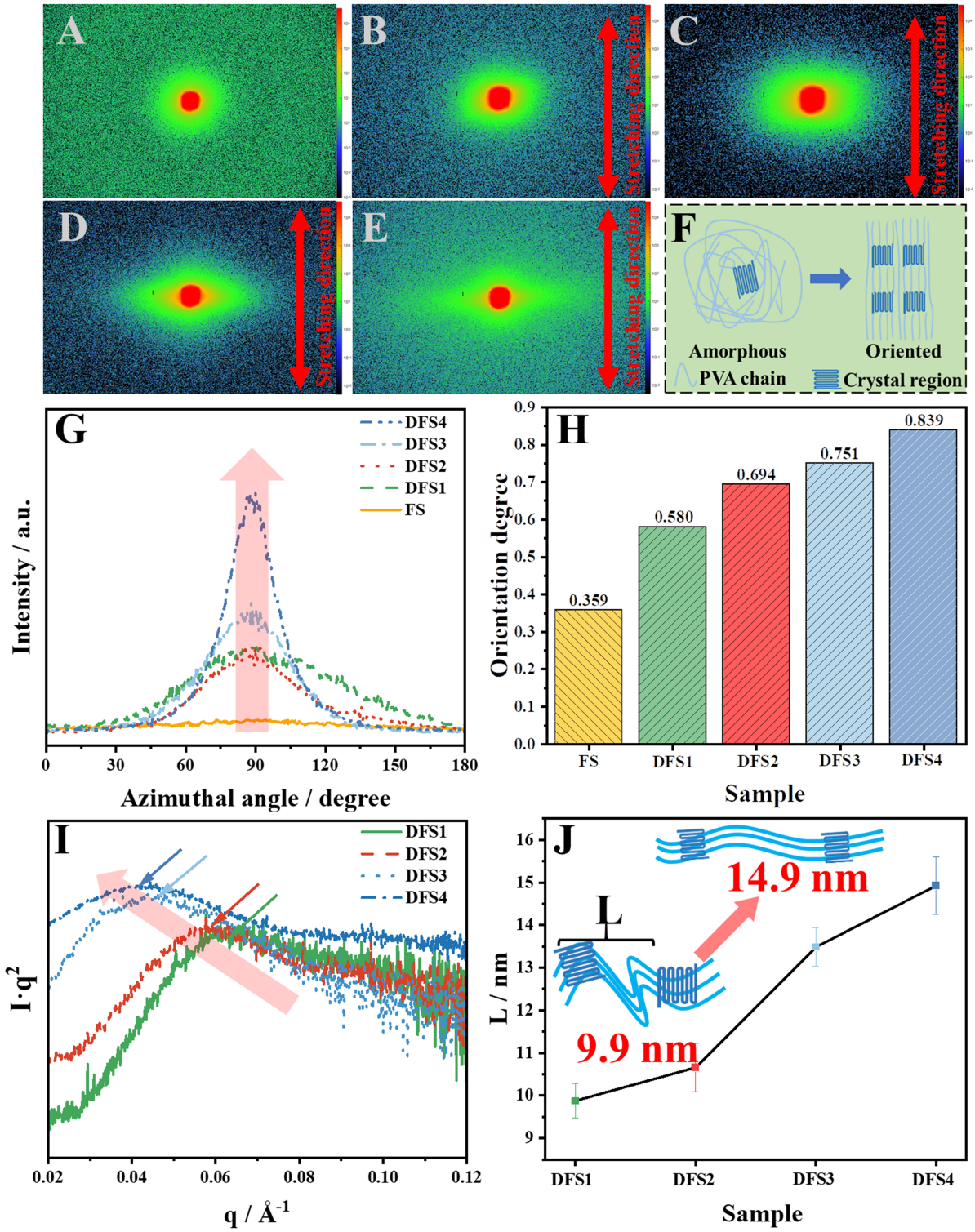

Figure 5. 2D-SAXS patterns of FS (A) and DFS PVA hydrogels with stretching ratios of 1 (B), 2 (C), 3 (D), and 4 (E); schematic diagram of microstructural changes from FS to DFS PVA hydrogel (F); scattering intensity *vs.* azimuthal angle curve of FS PVA and DFS PVA hydrogels (G) and corresponding orientation degree (H); scattering intensity $I \cdot q^2$ *vs.* scattering vector q along the orientation direction of DFS PVA hydrogels (I) and average distance L between adjacent crystal domains along the orientation direction *vs.* stretching ratio for DFS PVA hydrogels (J). SAXS: Small angle X-ray scattering; FS: frozen-salted out; DFS: directional freezing and salting-out; PVA: polyvinyl alcohol.

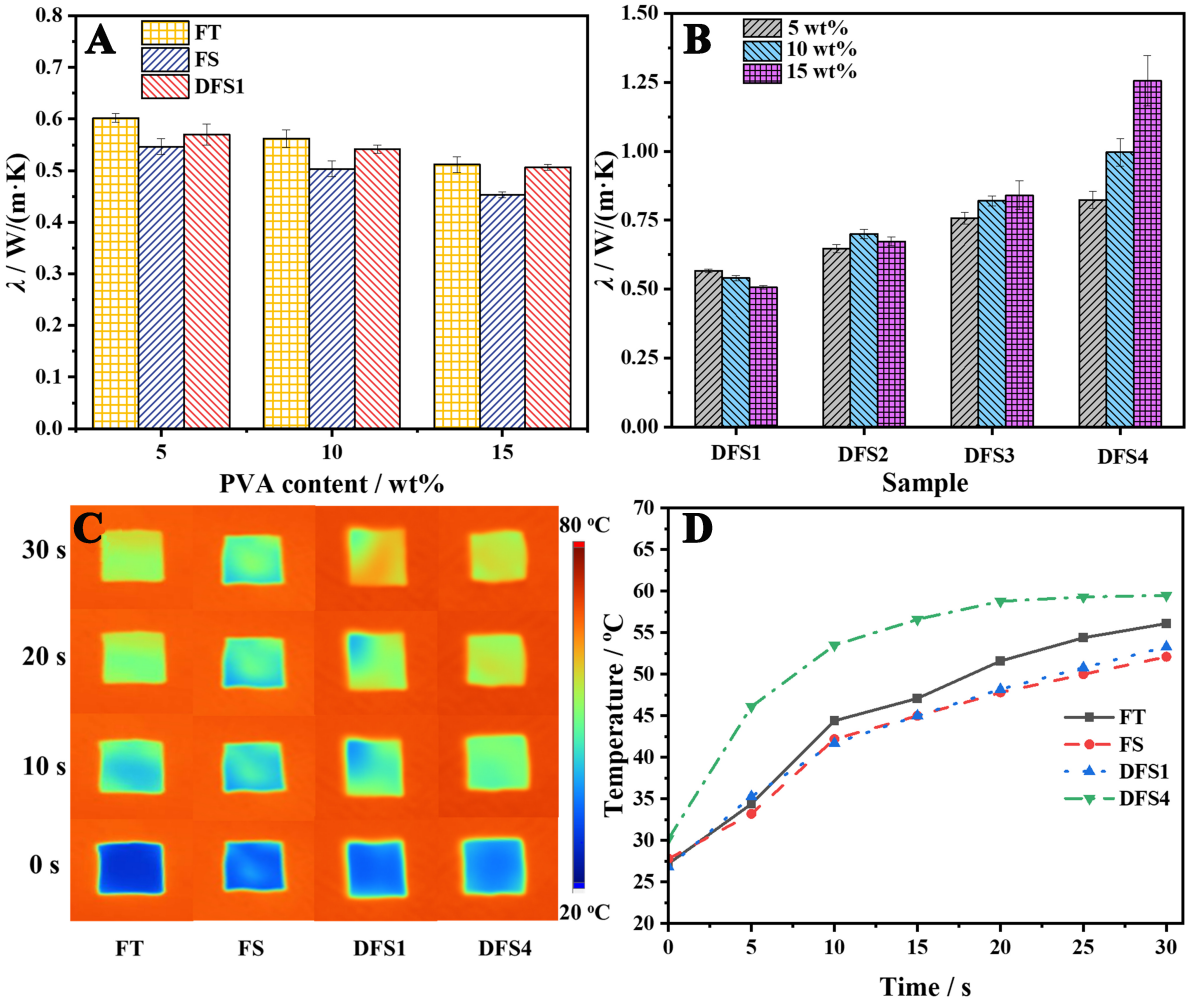

Figure 6. λ values of FT, FS, and DFS1 PVA hydrogels with different PVA mass fractions (A) and DFS PVA hydrogels with different PVA mass fractions and stretching ratios (B); infrared thermal images of FT, FS, DFS1, and DFS4 PVA hydrogels (C) and the corresponding surface temperatures (D) at different heating times. FT: Frozen-thawed; FS: frozen-salted out; PVA: polyvinyl alcohol.

5 wt%, the λ of the FT PVA hydrogel was 0.60 W/(m·K), higher than 0.55 and 0.57 W/(m·K) for FS and DFS1 PVA hydrogels, respectively. As the fraction of PVA increased further to 15 wt%, the λ of the FT PVA hydrogel decreased to 0.52 W/(m·K), which was almost equal to 0.51 W/(m·K) for DFS1 PVA hydrogel but higher than 0.45 W/(m·K) for FS PVA hydrogels.

This is because the PVA molecular chain had little effect on the intrinsic λ of the hydrogel at a low degree of orientation, and the thermal conduction was mainly through the motion collision of water molecules. Besides, the salting out process caused the aggregation of PVA chains, which would restrict the movement of water molecules, thereby reducing the λ of the hydrogel. Consequently, the λ of FS PVA hydrogels was lower than that of FT PVA hydrogels. However, the PVA chains in DFS1 PVA hydrogels were aligned along the ice crystal growth direction, leading to a reduced disordered structure[51], which facilitated heat transfer, thus showing a higher λ compared to FS PVA hydrogel. Although the λ of DFS1 PVA hydrogels was lower than that of FT PVA hydrogels, this difference decreased with increasing PVA mass fraction. This is because, although the orientation degree of PVA chains was increased in DFS1 PVA hydrogels, the low

PVA mass fraction showed little impact on the λ of the hydrogel. At the same time, due to the enhanced aggregation of PVA chains, the heat transfer of water molecules was limited, resulting in its λ being lower than that of FT PVA hydrogels. However, when the mass fraction of PVA increased, the oriented PVA chains in DFS1 PVA hydrogels significantly improved the λ, reducing the difference between the λ of DFS1 and FT PVA hydrogels.

Figure 6B displayed the λ of DFS PVA hydrogels at different PVA fractions and stretching ratios. At the same mass fraction of PVA, the λ of DFS PVA hydrogels gradually increased with the stretching ratio. The higher the PVA content was, the greater the enhancement of λ with increasing stretching ratios. When the PVA mass fraction was 15 wt%, DFS4 PVA hydrogels exhibited the highest λ of 1.25 W/(m·K), which was 145.1% higher than 0.51 W/(m·K) of DFS1 PVA hydrogel, and was also higher than 0.99 and 0.82 W/(m·K) of DFS4 PVA hydrogels with 5 wt% and 10 wt% of PVA, respectively. This is because the network of PVA hydrogels comprised crystalline and amorphous regions. The PVA chains were oriented and arranged under the effect of tension during stretching, and the orientation degree along the stretching direction increased with the increase of stretching ratio, which caused the increase of crystallinity. The orientation arrangement of PVA chains also increased the orderliness of amorphous domains. Besides, stretching caused aggregation of PVA chains, which enhanced the interaction between molecular chains. In addition, the salting-out effect caused strong hydrogen-bonding interactions between hydroxyl groups, which generated rigid cross-linking points and reduced ineffective molecular vibrations. These factors jointly restricted phonon scattering and segmental rotation. Therefore, the mean free path of phonons was increased and resulted in high-speed phonon propagation, facilitating more effective heat transfer[52-56] [Supplementary Figure 5]. The higher the mass fraction of PVA was, the greater the contribution of orderly orientated PVA chains to the overall λ of the hydrogel.

The infrared thermal imaging in Figure 6C provided an intuitive demonstration of the λ of different PVA hydrogels. As observed, the DFS4 PVA hydrogel exhibited the highest rate of temperature increase [Figure 6D], while the FS PVA hydrogel showed the lowest. The surface temperature of DFS4 PVA hydrogels reached 59.5 °C after 30 s, higher than 52.1 °C of FS PVA hydrogels, confirming DFS4 PVA hydrogels possessed the highest λ.

Mechanical properties of DFS PVA hydrogels

Figure 7A-F demonstrates that both FT PVA and FS PVA hydrogels exhibited typical stress-strain behavior, characterized by being "soft yet tough" with low modulus and high elongation at break. The tensile strength and toughness of FT PVA hydrogels improved gradually with the PVA mass fraction, while the elongation at break first increased and then decreased [Figure 7B]. As the mass fraction of PVA rose from 5 wt% to 15 wt%, the tensile strength of FT PVA hydrogel grew from 0.1 to 0.4 MPa whereas the elongation at break decreased from 240% to 215%. Besides, the toughness and the elastic modulus progressed from 0.09 MJ·m^{-3} and 0.03 MPa to 0.32 MJ·m^{-3} and 0.07 MPa, respectively [Figure 7C]. This is because higher PVA content effectively enhanced the aggregation of polymer chains, strengthening the interaction between molecular chains, thus improving breaking strength. Moderate physical entanglement between PVA chains can enhance the elongation at break, while excessive entanglement would reduce it. For the FS PVA hydrogels [Figure 7D], the tensile strength, toughness, and elastic modulus increased gradually with increasing the PVA content, whereas the elongation at break gradually decreased [Figure 7E and F]. When the mass fraction of PVA shifted from 5 wt% to 15 wt%, the tensile strength, toughness, and elastic modulus went from 0.8 MPa, 0.8 MJ·m^{-3}, and 0.3 MPa to 4.9 MPa, 4.8 MJ·m^{-3}, and 3.1 MPa, respectively, while the elongation at break dropped from 230% to 181%.

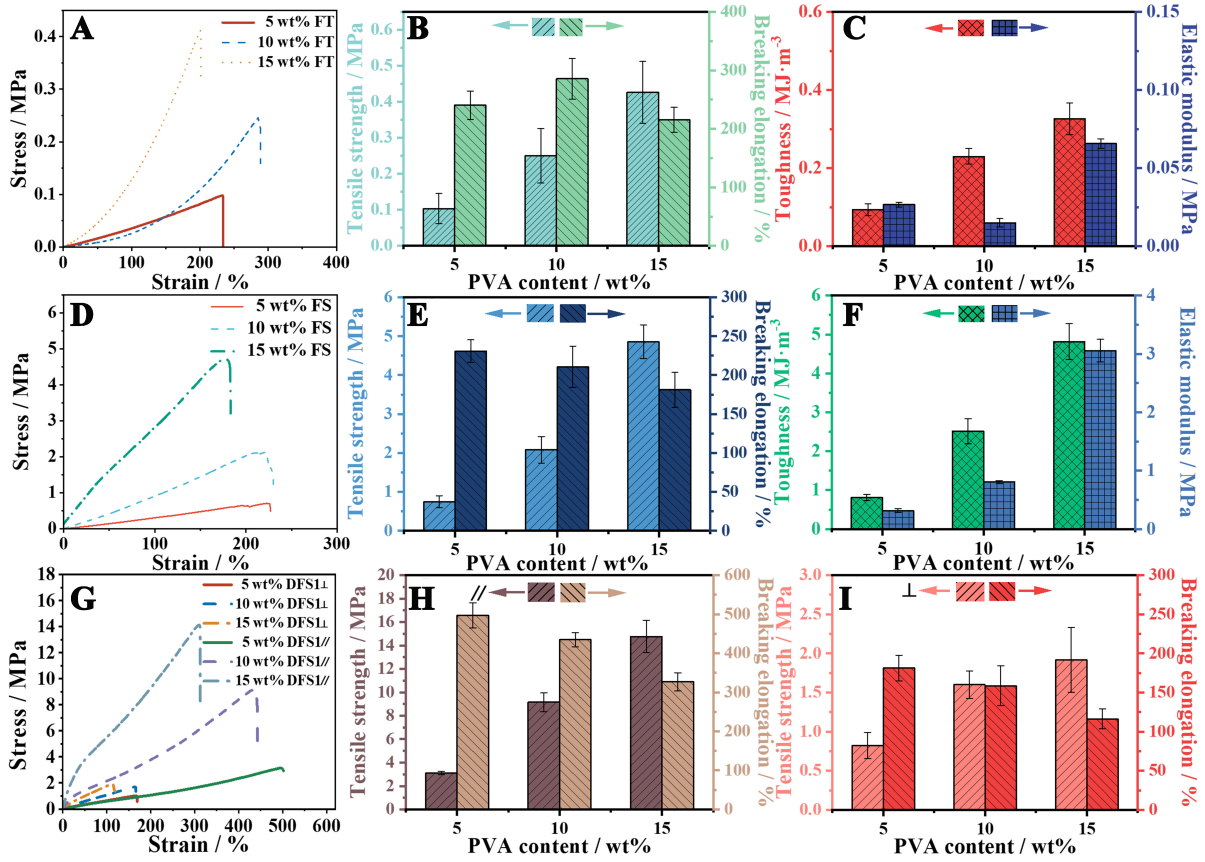

Figure 7. Stress-strain curves and mechanical properties of FT PVA (A-C), FS PVA (D-F), and DFS PVA (G-I, with stretching ratio of 1) hydrogels with different mass fractions of PVA. FT: Frozen-thawed; PVA: polyvinyl alcohol; FS: frozen-salted out; DFS: directional freezing and salting-out.

It can be concluded that FS PVA hydrogels possessed much higher tensile strength, toughness, and elastic modulus compared to FT PVA hydrogels. This is because, in FT PVA hydrogels, the polymer network was cross-linked only by a limited number of hydrogen bonds and physical entanglements, resulting in low tensile strength and poor toughness. However, during the salting-out process, the Hofmeister effect enhanced the aggregation of PVA chains, hydrogen bonding, and crystallinity of the hydrogel, leading to a densification of the polymer network and an obvious improvement in the tensile strength, toughness, and elastic modulus of PVA. However, the unordered distribution of crystalline and amorphous domains resulted in the non-uniform structure of FS PVA hydrogel, which caused the decrease of elongation at break.

The DFS PVA hydrogels exhibited a highly anisotropic character ascribed to the stretching-induced PVA chain alignment. In order to analyze this anisotropic behavior, the mechanical properties of DFS1 PVA hydrogels along and perpendicular to the stretching direction were examined. As displayed in Figure 7G, DFS1 PVA hydrogels were demonstrated to be strong, tough, and stretchable along the orientation direction but non-stretchable and brittle along the perpendicular direction because the tensile strength and elongation at break were much higher along the stretching direction.

Generally, tensile strength both along and perpendicular to the stretching direction rose, while the elongation at break decreased as the mass fraction of PVA increased [Figure 7H and I]. When the PVA content was 15 wt%, the tensile strength of DFS1 PVA hydrogel along the orientation direction increased to 14.8 MPa while the elongation at break decreased to 326.7%, which were significantly higher than the tensile strength (1.92 MPa) and elongation at break (116.3%) of perpendicular to the stretching direction. In addition, DFS1 PVA hydrogels displayed higher tensile strength and elongation at break than both FT and FS PVA hydrogels with the same content of PVA. This is attributed to the anisotropic oriented pore channel structure of DFS1 PVA hydrogels. The PVA polymer chains were orderly aligned along the orientation direction with crystalline and amorphous domains alternately distributed in the network, imparting high strength to the hydrogel. In contrast, PVA hydrogels presented a layered structure in the perpendicular direction, with aggregated molecular chains separated by pore channels containing a large amount of water, resulting in weak interaction forces and making them prone to fracture.

The mechanical properties of DFS PVA hydrogels with different mass fractions of PVA under various stretching ratios were also investigated [Figure 8]. As observed, the tensile strength of DFS PVA hydrogels with the same PVA mass fraction progressively increased with the stretching ratio, while the elongation at break gradually decreased. Meanwhile, the tensile strength of DFS PVA hydrogels with the same stretching ratio enhanced with the PVA mass fraction. Specifically, the tensile strength of DFS PVA hydrogels with 15 wt% PVA and a stretching ratio of 4 rose to 27.1 MPa from 14.8 MPa at a stretching ratio of 1, which was also much higher than the tensile strengths of 17.2 and 14.1 MPa for DFS PVA hydrogels with 5 wt% and 10 wt% of PVA, respectively, at a stretching ratio of 4. However, its elongation at break declined from 326.7% for a stretching ratio of 1 to 163.1%, yet remained higher than 121% and 125% of DFS PVA hydrogels with 5 wt% and 10 wt% PVA at a stretching ratio of 4. Additionally, its toughness and elastic modulus increased from 19.6 $MJ \cdot m^{-3}$ and 10.5 MPa at a stretching ratio of 1 to 25.3 $MJ \cdot m^{-3}$ and 21.5 MPa, respectively, both higher than 12.1 and 12.9 $MJ \cdot m^{-3}$ as well as 11.7 and 13.5 MPa for DFS PVA hydrogels with 5 wt% and 10 wt% PVA at a stretching ratio of 4.

This is attributed to the lower orientation and crystallinity of PVA chains within the hydrogel without stretching, resulting in lower tensile strength but larger deformation. Upon stretching, the PVA polymer chains were rearranged and aligned along the stretching direction. Furthermore, the polymer chains achieved higher orientation and crystallinity as the stretching ratio increased, leading to a more compact structure. The crystalline domains, which acted as a reinforcement phase, greatly enhanced the tensile strength. However, the movement of polymer chains would also be restricted, thereby reducing the elongation at break. The high mechanical strength of DFS PVA hydrogels can also be demonstrated by holding the weight of 500 g [Supplementary Figure 6A]. Additionally, these hydrogels demonstrated exceptional flexibility by undergoing arbitrary bending and folding as illustrated in Supplementary Figure 6B and C. Overall, the DFS PVA hydrogels exhibited both enhanced intrinsic thermal conductivities and mechanical properties compared to FT PVA hydrogels [Supplementary Table 1].

CONCLUSIONS

In summary, highly thermally conductive, strong, and tough PVA (DFS PVA) hydrogels with structural anisotropy were prepared through the synergy of directional freezing and mechanical stretching assisted by the Hofmeister effect. The DFS PVA hydrogel with 15 wt% of PVA and a stretching ratio of 4 (DFS4) exhibited the highest λ of 1.25 W/(m·K), which was 2.4 and 2.8 times that of 0.52 and 0.45 W/(m·K) for hydrogels made by FT and FS methods, respectively. Meanwhile, the DFS4 PVA hydrogels with 15 wt% PVA also exhibited greatly enhanced mechanical performances. For instance, their tensile strength, toughness, and elastic modulus significantly increased to 27.1 MPa, 25.3 $MJ \cdot m^{-3}$, and 21.5 MPa, respectively,

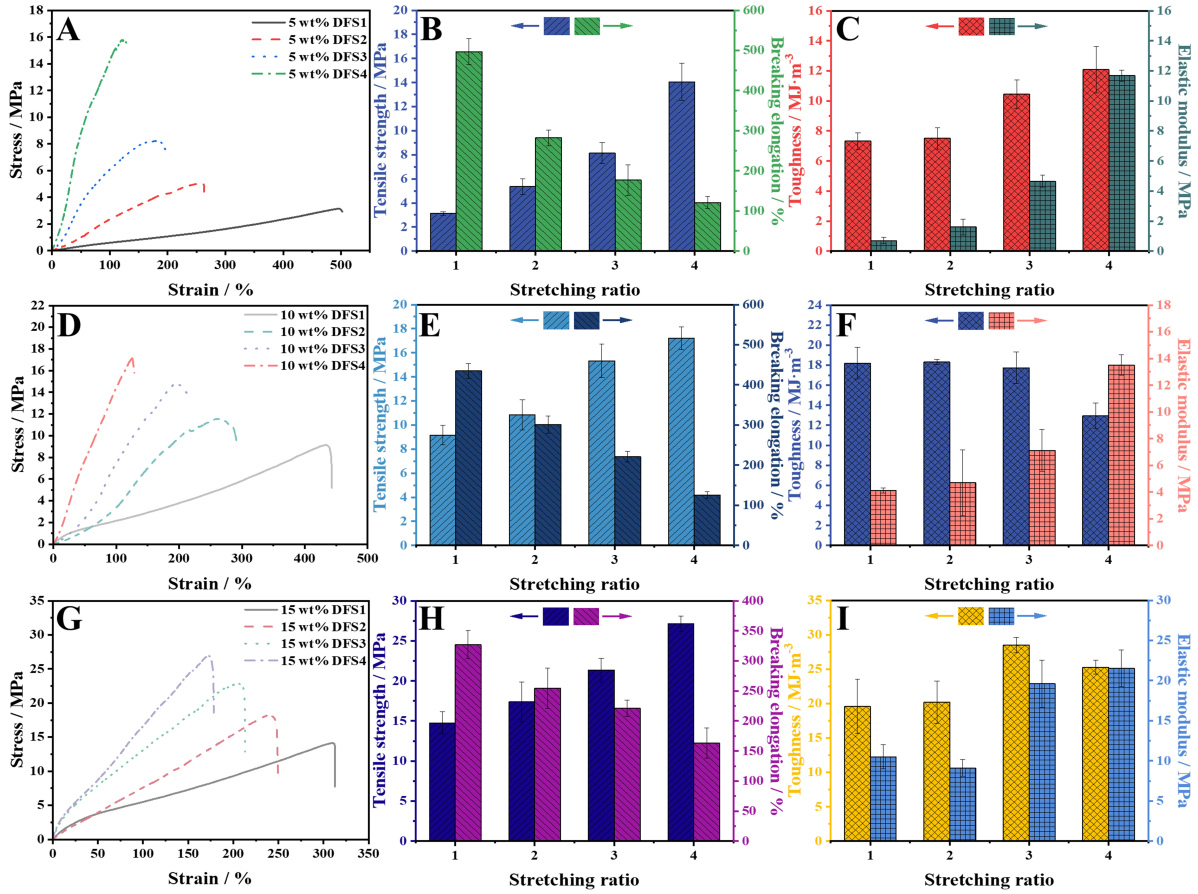

Figure 8. Stress-strain curves and mechanical properties of DFS PVA hydrogels at different stretching ratios with 5 wt% (A-C), 10 wt% (D-F), and 15 wt% (G-I) of PVA. DFS: Directional freezing and salting-out; PVA: polyvinyl alcohol.

from 0.4 MPa, 0.32 MJ·m^{-3}, and 0.07 MPa for FT PVA hydrogels. Additionally, the elongation at break was 163.1%. This enhancement was attributed to the salting-out effect, which generated hydrophobic and crystalline regions, while directional freezing and stretching promoted chain orientation in the DFS strategy. These effects synergistically contributed to the improvement of intrinsic λ and mechanical properties of PVA hydrogels. This study provides a new strategy for simultaneously enhancing intrinsic λ and mechanical properties of hydrogels by constructing an oriented structure with alternating soft (PVA chains) and hard (physical cross-linking) regions. This strategy is expected to promote the application of PVA hydrogels in bioengineering and flexible electronics. Future work will focus on introducing stimuli-responsive materials or dynamic covalent bonds into the hydrogels. For instance, integrating carbon nanotubes will impart photo-thermal effect to PVA hydrogels under near-infrared light, which could be utilized for wound healing by remote and non-contact control. Additionally, introducing dynamic covalent bonds into the hydrogel network could endow the hydrogel with self-healing behavior triggered by external stimuli.

DECLARATIONS

Authors' contributions

Conceptualization, data curation, investigation, methodology, analysis, writing - original draft, writing - review and editing: Zhang, J.; Tang, C.

Data analysis, writing - review and editing: Kong, Q.; He, M.; Lv, P.; Guo, H.; Guo, Y.; Shi, X.

Conceptualization, funding acquisition, project administration, supervision, writing - review and editing: Zhang, J.; Gu, J.

Availability of data and materials

The data presented in this study is available upon request from the corresponding author.

Financial support and sponsorship

This work was supported by the National Natural Science Foundation of China (52473084), Natural Science Basic Research Program of Shaanxi (2024JC-TBZC-04), the Innovation Capability Support Program of Shaanxi (2024RS-CXTD-57), Natural Science Basic Research Plan in Shaanxi Province of China (2024JC-YBMS-279), and the Analytical & Testing Center of Northwestern Polytechnical University for SEM test performed in this work.

Conflicts of interest

Gu, J. is listed as an Associate Editor of the journal *Soft Science*. However, Gu, J. was not involved in any steps of the editorial process, including reviewer selection, manuscript handling, or decision-making. The other authors declare that there are no conflicts of interest.

Ethical approval and consent to participate

Not applicable.

Consent for publication

Not applicable.

REFERENCES

1. Zhang, Y. S.; Khademhosseini, A. Advances in engineering hydrogels. *Science* **2017**, *356*, eaaf3627. DOI PubMed PMC
2. Ke, X.; Mu, X.; Chen, S.; et al. Reduced graphene oxide reinforced PDA-Gly-PVA composite hydrogel as strain sensors for monitoring human motion. *Soft. Sci.* **2023**, *3*, 1-12. DOI
3. Wu, Y.; Zhang, Y.; Wu, H.; et al. Solvent-exchange-assisted wet annealing: a new strategy for superstrong, tough, stretchable, and anti-fatigue hydrogels. *Adv. Mater.* **2023**, *35*, e2210624. DOI
4. Kim, S. D.; Park, K.; Lee, S.; et al. Injectable and tissue-conformable conductive hydrogel for MRI-compatible brain-interfacing electrodes. *Soft. Sci.* **2023**, *3*, 18. DOI
5. Xu, Q.; Wu, Z.; Zhao, W.; et al. Strategies in the preparation of conductive polyvinyl alcohol hydrogels for applications in flexible strain sensors, flexible supercapacitors, and triboelectric nanogenerator sensors: an overview. *Adv. Compos. Hybrid. Mater.* **2023**, *6*, 783. DOI
6. Liu, D.; Cao, Y.; Jiang, P.; et al. Tough, transparent, and slippery PVA hydrogel led by syneresis. *Small* **2023**, *19*, e2206819. DOI
7. Lei, D.; Xiao, Y.; Shao, L.; Xi, M.; Jiang, Y.; Li, Y. Dual-stimuli-responsive and anti-freezing conductive ionic hydrogels for smart wearable devices and optical display devices. *ACS. Appl. Mater. Interfaces.* **2023**, *15*, 24175-85. DOI
8. Jing, L.; Li, H.; Tay, R. Y.; et al. Biocompatible hydroxylated boron nitride nanosheets/poly(vinyl alcohol) interpenetrating hydrogels with enhanced mechanical and thermal responses. *ACS. Nano.* **2017**, *11*, 3742-51. DOI
9. Zhao, L.; Zhang, J.; Cao, P.; et al. Fast water transport reversible CNT/PVA hybrid hydrogels with highly environmental tolerance for multifunctional sport headband. *Compos. Part. B. Eng.* **2021**, *211*, 108661. DOI
10. Wu, S.; Hua, M.; Alsaid, Y.; et al. Poly(vinyl alcohol) hydrogels with broad-range tunable mechanical properties via the hofmeister effect. *Adv. Mater.* **2021**, *33*, e2007829. DOI
11. Chen, X.; Wu, K.; Zhang, Y.; Liu, D.; Li, R.; Fu, Q. Tropocollagen-inspired hierarchical spiral structure of organic fibers in epoxy bulk for 3D high thermal conductivity. *Adv. Mater.* **2022**, *34*, e2206088. DOI
12. Yang, J.; Shen, X.; Yang, W.; Kim, J. Templating strategies for 3D-structured thermally conductive composites: recent advances and thermal energy applications. *Prog. Mater. Sci.* **2023**, *133*, 101054. DOI
13. Ren, L.; Guo, H.; Kang, L.; Niu, H.; Lv, R.; Bai, S. Lightweight, electrical insulating, and high thermally conductive all-polymer composites with reinforced interfaces. *Compos. Sci. Technol.* **2023**, *240*, 110080. DOI

14. Guo, C.; He, L.; Yao, Y.; et al. Bifunctional liquid metals allow electrical insulating phase change materials to dual-mode thermal manage the Li-ion batteries. *Nano-Micro Lett.* **2022**, *14*, 202. DOI PubMed PMC
15. Yun, J. Recent progress in thermal management for flexible/wearable devices. *Soft. Sci.* **2023**, *3*, 12. DOI
16. Zhang, H.; Guo, Y.; Zhao, Y.; et al. Liquid crystal-engineered polydimethylsiloxane: enhancing intrinsic thermal conductivity through high grafting density of mesogens. *Angew. Chem. Int. Ed.* **2025**, e202500173. DOI
17. Lin, Y.; Kang, Q.; Liu, Y.; et al. Flexible, highly thermally conductive and electrically insulating phase change materials for advanced thermal management of 5G base stations and thermoelectric generators. *Nano-Micro Lett.* **2023**, *15*, 31. DOI PubMed PMC
18. He, M.; Zhong, X.; Lu, X.; et al. Excellent low-frequency microwave absorption and high thermal conductivity in polydimethylsiloxane composites endowed by hydrangea-like CoNi@BN heterostructure fillers. *Adv. Mater.* **2024**, *36*, e2410186. DOI
19. Miao, D.; Cheng, N.; Wang, X.; Yu, J.; Ding, B. Integration of Janus wettability and heat conduction in hierarchically designed textiles for all-day personal radiative cooling. *Nano. Lett.* **2022**, *22*, 680-7. DOI
20. Zhang, F.; Zhang, J.; Zhang, K.; et al. Highly thermally conductive liquid crystalline epoxy resin vitrimers with reconfigurable, shape-memory, photo-thermal, and closed-loop recycling performance. *Adv. Sci.* **2025**, *12*, e2410362. DOI PubMed PMC
21. Guo, Y.; Wang, S.; Zhang, H.; et al. Consistent thermal conductivities of spring-like structured polydimethylsiloxane composites under large deformation. *Adv. Mater.* **2024**, *36*, e2404648. DOI
22. Qin, M.; Huo, Y.; Han, G.; et al. Three-dimensional boron nitride network/polyvinyl alcohol composite hydrogel with solid-liquid interpenetrating heat conduction network for thermal management. *J. Mater. Sci. Technol.* **2022**, *127*, 183-91. DOI
23. Tian, R.; Jia, X.; Bai, Y.; Yang, J.; Song, H. Fluorinated graphene thermally conductive hydrogel with a solid-liquid interpenetrating heat conduction network. *ACS. Appl. Mater. Interfaces.* **2024**, *16*, 1451-60. DOI
24. Kazimierska-Drobny, K.; El, F. M.; Kaczmarek, M. Determination of mechanical and hydraulic properties of PVA hydrogels. *Mater. Sci. Eng. C. Mater. Biol. Appl.* **2015**, *48*, 48-54. DOI PubMed
25. Li, W.; Qiao, K.; Zheng, Y.; et al. Preparation, mechanical properties, fatigue and tribological behavior of double crosslinked high strength hydrogel. *J. Mech. Behav. Biomed. Mater.* **2022**, *126*, 105009. DOI
26. Duan, S.; Shi, Q.; Hong, J.; et al. Water-modulated biomimetic hyper-attribute-gel electronic skin for robotics and skin-attachable wearables. *ACS. Nano.* **2023**, 1355-71. DOI
27. Ji, D.; Liu, P.; Im, P.; Shin, S.; Kim, J. Thermal interface hydrogel composites mechanically compliant with curvy skins and rigid electronic modules. *Adv. Funct. Mater.* **2024**, *34*, 2402144. DOI
28. Xu, S.; Cai, S.; Liu, Z. Thermal conductivity of polyacrylamide hydrogels at the nanoscale. *ACS. Appl. Mater. Interfaces.* **2018**, *10*, 36352-60. DOI
29. Zhang, Z.; Tan, S.; Bao, Z.; Wu, Y.; Wang, C. Thermal conductivity of PNIPAm hydrogels and heat management as smart windows. *Macro. Mater. Eng.* **2023**, *308*, 2200566. DOI
30. Zhang, M.; Yang, Y.; Li, M.; et al. Toughening double-network hydrogels by polyelectrolytes. *Adv. Mater.* **2023**, *35*, e2301551. DOI
31. Singh, V.; Bougher, T. L.; Weathers, A.; et al. High thermal conductivity of chain-oriented amorphous polythiophene. *Nat. Nanotechnol.* **2014**, *9*, 384-90. DOI
32. Tu, H.; Xie, K.; Lin, X.; et al. Superior strength and highly thermoconductive cellulose/boron nitride film by stretch-induced alignment. *J. Mater. Chem. A.* **2021**, *9*, 10304-15. DOI
33. Candadai, A. A.; Weibel, J. A.; Marconnet, A. M. Thermal conductivity of ultrahigh molecular weight polyethylene: from fibers to fabrics. *ACS. Appl. Polym. Mater.* **2020**, *2*, 437-47. DOI
34. Zhang, Y.; Ruan, K.; Zhou, K.; Gu, J. Controlled distributed $Ti_3C_2T_x$ hollow microspheres on thermally conductive polyimide composite films for excellent electromagnetic interference shielding. *Adv. Mater.* **2023**, *35*, e2211642. DOI
35. Han, Y.; Ruan, K.; He, X.; et al. Highly thermally conductive aramid nanofiber composite films with synchronous visible/infrared camouflages and information encryption. *Angew. Chem. Int. Ed.* **2024**, *63*, e202401538. DOI
36. Uetani, K.; Okada, T.; Oyama, H. T. In-plane anisotropic thermally conductive nanopapers by drawing bacterial cellulose hydrogels. *ACS. Macro. Lett.* **2017**, *6*, 345-9. DOI PubMed
37. Wu, T.; Zhu, J.; Yu, H.; Qu, S.; Yang, W. Stretch induced thermal conduction anisotropy of hydrogel. *Int. J. Heat. Mass. Transfer.* **2022**, *185*, 122445. DOI
38. Lin, S.; Liu, J.; Liu, X.; Zhao, X. Muscle-like fatigue-resistant hydrogels by mechanical training. *Proc. Natl. Acad. Sci. U. S. A.* **2019**, *116*, 10244-9. DOI PubMed PMC
39. Chen, Y.; Sun, X.; Luo, L.; et al. Super strong and tough PVA hydrogel fibers based on an ordered-to-disordered structural construction strategy targeting artificial ligaments. *Adv. Funct. Mater.* **2024**. DOI
40. Mredha, M. T. I.; Guo, Y. Z.; Nonoyama, T.; Nakajima, T.; Kurokawa, T.; Gong, J. P. A facile method to fabricate anisotropic hydrogels with perfectly aligned hierarchical fibrous structures. *Adv. Mater.* **2018**, *30*, 1704937. DOI PubMed
41. Gu, L.; Jiang, Y.; Hu, J. Scalable spider-silk-like supertough fibers using a pseudoprotein polymer. *Adv. Mater.* **2019**, *31*, e1904311. DOI PubMed
42. Wang, W.; Wang, Y.; Zheng, J.; et al. A vasculatural hydrogel combined with Prussian blue for solar-driven vapor generation. *J. Mater. Chem. A.* **2022**, *10*, 12608-15. DOI
43. Zhang, L.; Wang, K.; Weng, S.; Jiang, X. Super strong and tough anisotropic hydrogels through synergy of directional freeze-casting, metal complexation and salting out. *Chem. Eng. J.* **2023**, *463*, 142414. DOI

44. Mredha, M. T. I.; Le, H. H.; Tran, V. T.; Trtik, P.; Cui, J.; Jeon, I. Anisotropic tough multilayer hydrogels with programmable orientation. *Mater. Horiz.* **2019**, *6*, 1504-11. DOI
45. Wei, W. Hofmeister effects shine in nanoscience. *Adv. Sci.* **2023**, *10*, e2302057. DOI PubMed PMC
46. Lo Nostro P, Ninham BW. Hofmeister phenomena: an update on ion specificity in biology. *Chem. Rev.* **2012**, *112*, 2286-322. DOI PubMed
47. Zou, H.; Meng, X.; Zhao, X.; Qiu, J. Hofmeister effect-enhanced hydration chemistry of hydrogel for high-efficiency solar-driven interfacial desalination. *Adv. Mater.* **2023**, *35*, e2207262. DOI
48. Sun, X.; Mao, Y.; Yu, Z.; Yang, P.; Jiang, F. A biomimetic "salting out-alignment-locking" tactic to design strong and tough hydrogel. *Adv. Mater.* **2024**, *36*, e2400084. DOI
49. Lin, X.; Zhang, X.; Nie, Z.; et al. A highly aligned X-shaped hydrogel fiber via cooperative roles of amorphous and crystalline network mediated by Hofmeister effect. *Polymer* **2024**, *292*, 126538. DOI
50. He, Q.; Huang, Y.; Wang, S. Hofmeister effect-assisted one step fabrication of ductile and strong gelatin hydrogels. *Adv. Funct. Mater.* **2018**, *28*, 1705069. DOI
51. Zhang, J.; Dang, L.; Zhang, F.; Zhang, K.; Kong, Q.; Gu, J. Effect of the structure of epoxy monomers and curing agents: toward making intrinsically highly thermally conductive and low-dielectric epoxy resins. *JACS Au.* **2023**, *3*, 3424-35. DOI PubMed PMC
52. Rodríguez-Martínez, X.; Saiz, F.; Dörling, B.; et al. On the thermal conductivity of conjugated polymers for thermoelectrics. *Adv. Energy. Mater.* **2024**, *14*, 2401705. DOI
53. Wang, Z.; Wu, Z.; Weng, L.; et al. A roadmap review of thermally conductive polymer composites: critical factors, progress, and prospects. *Adv. Funct. Mater.* **2023**, *33*, 2301549. DOI
54. Yuan, S. J.; Peng, Z. Q.; Rong, M. Z.; Zhang, M. Q. Enhancement of intrinsic thermal conductivity of liquid crystalline epoxy through the strategy of interlocked polymer networks. *Mater. Chem. Front.* **2022**, *6*, 1137-49. DOI
55. Hossain, M. M.; Olamilekan, A. I.; Jeong, H.; et al. Diacetylene-containing dual-functional liquid crystal epoxy resin: strategic phase control for topochemical polymerization of diacetylenes and thermal conductivity enhancement. *Macromolecules* **2022**, *55*, 4402-10. DOI
56. He, M.; Zhang, L.; Ruan, K.; et al. Functionalized aluminum nitride for improving hydrolysis resistances of highly thermally conductive polysiloxane composites. *Nano-Micro Lett.* **2025**. DOI